EXPERIMENTAL IDENTIFICATION OF FORCE-DISPLACEMENT BEHAVIOR FOR PASSIVE DAMPERS IN A FOUR STORY, REINFORCED CONCRETE, "SMART" BASE-ISOLATED STRUCTURE

P.T. Brewick[(1)], E.A. Johnson[(2)], and R.E. Christenson[(3)]

[(1)] *Postdoctoral Fellow, University of Southern California, brewick@usc.edu*
[(2)] *Professor, University of Southern California, JohnsonE@usc.edu*
[(3)] *Professor, University of Connecticut, rchriste@engr.uconn.edu*

Abstract

In this paper, the force and displacement sensing data from full-scale experimental tests of a base-isolated structure are analyzed to create a model for the hysteretic behavior observed in the isolators; the intent is that this model could be used for future nonlinear finite element studies and simulations. Displacement data is available in both of the horizontal planar directions of the motion, meaning that the hysteric force will be bi-axial and, thus, modeled by coupled nonlinear differential equations. A Bouc-Wen model was assumed for parameter fitting. Identification was first performed using the random base motions; however, it was revealed that the amplitudes of motion were small enough that the isolators exhibited generally linear behavior. A series of tests were also conducted in which the input intensity of both historical and synthetic earthquakes was gradually increased. Due to the well-documented amplitude dependence of nonlinear phenomena, the tests with the largest input amplitudes were using for identification; the resulting parameters were applied to the lower intensity tests to evaluate the model's ability to predict responses of different levels of excitation.

Keywords: large-scale experimental testing; nonlinear identification; hysteresis

1. Introduction

Seismic protective systems, such as base-isolation and passive damping devices, perform a vital function, mitigating a building's response to seismic input, thereby ensuring the safety of the building's occupants. These systems have been the focus of benchmark studies [1] and scaled experiments [2,3], but full-scale testing of buildings and structures incorporating these systems is much less common. The paucity of full-scale tests can be largely attributed to the immense costs associated with those experiments, but conducting tests in which large building specimens are subjected to earthquake excitations offers researchers a trove of valuable information about the building's dynamics. These tests become all the more necessary when innovative seismic protection systems are included in the building's design. The fact that the governing dynamics of these systems are often highly nonlinear creates a notable challenge when attempting to predict the building's response, particularly for excitations not included in the experimental testing regime, such as other hazardous natural excitations [4]; properly designing and calibrating models of base isolators that accurately capture the nonlinear behavior often proves extremely difficult. Further, different isolators and devices require their own unique models based on their governing physics and behavior. Additionally, bi-axial structural interaction has been shown to contribute significantly to the nonlinear response for structures under earthquake excitation [5].

The researchers at E-Defense (a part of the Japan's National Research Institute for Earth Science and Disaster Resilience, NIED), a unique facility capable of testing full-scale structures, designed and constructed a four-story base-isolated building to test and study, in part, the performance of the isolation layer when subjected to strong impulsive and long-period excitations [6]. This base-isolated building is particularly compelling because its isolation layer is non-homogeneous, as it is composed of several disparate devices: rubber bearings, elastic sliding bearings, passive metallic yielding dampers, and controllable oil dampers with solenoids. The structure was constructed in late 2012 and early 2013, and underwent initial testing in March 2013. A variety of sensors, including displacement and force transducers, were mounted within the isolation layer to measure its response to the shake table excitations. Subsequent August 2013 tests, on which this study is based, included both random base motions and historical and synthetic ground motions. The purpose of this study was to learn how the various devices performed under different excitations and to explore whether it is possible to build predictive models that accurately capture the devices' behaviors.

Modeling the behavior of passive base-isolation systems has been the subject of many recent studies [7], including those more specifically focused on lead-rubber bearings [8], sliding bearings [9], friction pendulum systems [10,11], rolling isolation [12], and metallic dampers [13,14]. Identification of nonlinear hysteretic systems may be tackled using either nonparametric [15] or parametric [16,17,18] techniques. This study seeks to create bi-axial models for the hysteresis observed in the sliding bearings and steel dampers during one of the simulated earthquake tests based on the nonlinear dynamic formulation originally presented in Nagarajaiah et al. [2]. These models are then applied to measurements from other tests, as well as the other devices, to determine their ability to serve as generalized models. The experimental set-up and identification methodology are presented first, followed by a discussion of the identification results. Conclusions and proposed avenues for future research are presented at the end.

2. Experimental Set-up

The test structure rests upon E-Defense's shake table, which has a six degree-of-freedom controller and is capable of three-dimensional seismic simulations [6]. The structure consists of a four story, asymmetric, moment frame with a setback and coupled transverse-torsional motion (Fig. 1). The 690-ton superstructure has dimensions of approximately 14m by 10m by 15m and was built to satisfy Japanese design code. As previously detailed, the building sits on an extensive passive base-isolation layer composed of rubber bearings, sliding bearings, passive steel dampers and oil dampers with solenoids. Tests conducted during a three-week span in August 2013, on which this study is based, included both random base motions and historical and synthetic ground motions; all but the very last day of testing featured the controllable dampers acting in a purely passive mode.

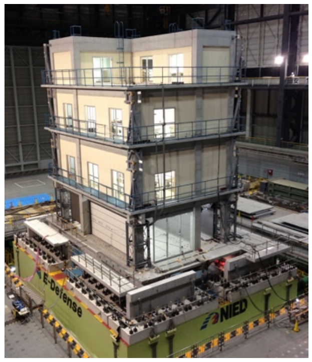

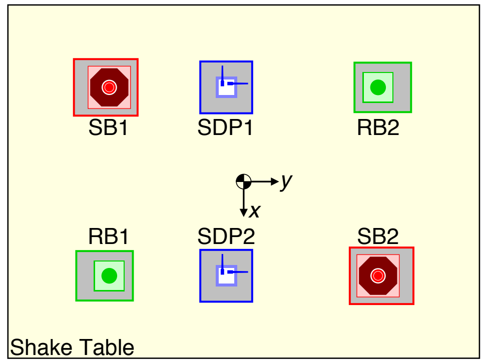

Fig. 1 – Elevation view (left) of E-Defense building used for testing and isolation-layer plan view (right)

The isolation layer was extensively instrumented, with sensors measuring differential displacements at eight locations (4 in each of the *X* and *Y* directions, respectively) and force transducers measuring the *X*, *Y* and *Z* directional components of the forces in each of the different isolation-layer devices. All sensors featured a sampling rate of 1 kHz; the signals were passed through a low-pass filter with a cutoff frequency of 35 Hz.

Numerous tests were conducted over that three-week span, but this study focuses on the first day of testing (8/8/2013). During these tests, the base-isolation layer was configured such that each type of device is used twice, for a total of six isolation-layer devices, *i.e.*, two rubber bearings (RB1 and RB2), two sliding bearings (SB1 and SB2), and two passive yielding steel damper pairs (SDP1 and SDP2), as shown in Fig. 1. The oil dampers were excluded from these initial tests. The first several tests (Tests 001 – 012) subjected the building to random excitation along different table axes, *i.e.*, *X*, *Y* and *Z* directions, and linear combinations thereof. Brief descriptions of the random excitation tests relevant to this study are given in Table 1.

Table 1 – Random excitation tests included in this study

Test No.	Brief Description
003	Random excitation along the *X* axis of shake table
004	Random excitation along the *Y* axis of shake table
010	Random excitation across all shake table DOFs

The next four tests (Tests 013 – 016) subjected the building to scaled versions of the March 2011 Mw9.0 Tohoku-Oki earthquake (K-NET Furukawa record), each with a duration of 315 seconds. As a means of comparing the relative intensity of the earthquake excitations from Tests 013 – 016, Table 2 presents the root-mean-square (RMS) of the accelerations measured on the shake table in its *X* and *Y* directions. The progression in RMS, and thus intensity, is obvious. The largest jump was observed from Test 013 to 014; Test 016 has the largest RMS values in both directions.

Table 2 – Comparison of RMS values measured on shake table for Tests 013 – 016

Sensor Dir.	Test 013	Test 014	Test 015	Test 016
X	25.87 cm/s^2	40.59 cm/s^2	39.15 cm/s^2	41.19 cm/s^2
Y	26.17 cm/s^2	41.26 cm/s^2	41.57 cm/s^2	43.25 cm/s^2

3. Identification Methodology

The displacement data includes both horizontal planar directions of table motion, *i.e.*, the *X*–*Y* plane; given an assumption of rigidity for the table, the displacement sensors can be used to find the generalized displacements, x, y and θ, across the isolation layer. Thus, the displacements for a given isolation-layer device at any location can then be computed, allowing for the restoring force–displacement behavior to be established in the x and y directions for each isolation-layer device, where "restoring force" is used herein to refer to the total measured force for a given isolation-layer device in a chosen direction. As the devices are governed by different physics, different models are needed for capturing and predicting the restoring force behaviors. These models are created using the force and displacement measurement data.

The behavior of the sliding bearing is governed by friction; one of the simplest friction-based models for a sliding bearing [19] is shown in Eq. (1)

$$q = \mu_{s} W_{SB\#} \operatorname{sgn}(\dot{u}) \tag{1}$$

where q is the restoring force, μ_s is the coefficient of sliding friction, $W_{SB\#}$ is the bearing pressure (weight) on the sliding bearing (SB1 or SB2), $\dot{u}$ is the velocity, and $\operatorname{sgn}(\cdot)$ is the sign (or signum) function. The expression in Eq. (1) is for uni-axial motion and would therefore be applied to either the motion in the x or y direction.

A more complex model for sliding bearings has been developed that takes into account both biaxial motion and hysteretic behavior [3]. Since the x and y components of both restoring forces and displacements are available, modeling the biaxial interaction is possible in this case and may be accomplished using coupled nonlinear differential equations. This modified model for biaxial interaction in the sliding bearings is shown in Eq. (2).

$$\begin{Bmatrix} q_x \\ q_y \end{Bmatrix} = \mu_s W_{SB\#} \begin{Bmatrix} Z_x \\ Z_y \end{Bmatrix} \tag{2}$$

where q_x and q_y are the restoring forces in the x and y directions, respectively, and Z_x and Z_y are the corresponding non-dimensional hysteretic variables. These hysteretic components are described by a Bouc-Wen model [20], which is subject to the following coupled first-order differential equations

$$D_y \dot{Z}_x = A\dot{u}_x - \beta\left|\dot{u}_x Z_x\right| Z_x - \gamma \dot{u}_x Z_x^2 - \beta\left|\dot{u}_y Z_y\right| Z_x - \gamma \dot{u}_y Z_x Z_y \tag{3}$$

$$D_y \dot{Z}_y = A\dot{u}_y - \beta\left|\dot{u}_y Z_y\right| Z_y - \gamma \dot{u}_y Z_y^2 - \beta\left|\dot{u}_x Z_x\right| Z_y - \gamma \dot{u}_x Z_x Z_y \tag{4}$$

where A, β and γ represent design parameters within the equations that control the shape of the hysteresis, D_y represents the yield displacement, and u_x and u_y are the responses in the x and y directions, respectively.

In contrast to the sliding bearing, elastic models better describe the observed behavior in the rubber bearings and steel dampers. As with the sliding bearing, the restoring forces will be modeled in a manner that captures the biaxial interaction and hysteretic behavior. Following the example in Park et al. [5], the restoring forces in either the rubber bearing or steel damper may be modeled using a system of equations

$$\begin{Bmatrix} q_x \\ q_y \end{Bmatrix} = \alpha\, \mathbf{K} \begin{Bmatrix} u_x \\ u_y \end{Bmatrix} + (1-\alpha)\, \mathbf{K}\, D_y \begin{Bmatrix} Z_x \\ Z_y \end{Bmatrix} \tag{5}$$

in which u_x and u_y are the displacements, α represents the post-yielding stiffness ratio, **K** is the initial stiffness matrix (of dimension 2 × 2) and Z_x and Z_y are the familiar hysteretic components of the response. As before, these hysteretic components are governed by the Bouc-Wen model.

The restoring forces and displacements are known for all devices; the velocities are estimated using a central finite difference of the displacements. The remaining coefficients and response quantities for the respective models were assumed unknown. The unknown model parameters (which differed between models) are identified using a nonlinear optimization scheme. The cost function for the optimization is shown in Eq. (6), where $\hat{q}_x$ and $\hat{q}_y$ represent the model-based estimates of the restoring forces and θ is the vector of unknown coefficients and parameters.

$$J = \sum_k \left[\hat{q}_x(k,\theta) - q_x(k)\right]^2 + \left[\hat{q}_y(k,\theta) - q_y(k)\right]^2 \tag{6}$$

4. Results and Discussion

4.1 Random excitation tests

As shown in Table 1, Test 003 subjected the base-isolated structure to random excitation along the *X* axis; thus, data recorded during this test can be used to establish preliminary estimates of the linear stiffness in the *x* direction for each of the isolation devices. Fig. 2 displays the restoring force-displacement relationships for one of each of the devices.

Stiffness estimates are included in Fig. 2 to better elucidate the differences between the devices, *e.g.*, the steel damper is clearly the stiffest device. Additional restoring force components, such as damping, are certainly present, especially for the steel dampers; however, only focusing on the stiffness component allows for that parameter to simply be tuned, instead of fully estimated, for the more complex hysteretic models. Following a similar procedure for Test 004 reveals very similar *y*–directional stiffness estimates, giving credence to the applicability of bi-directional models for these devices.

The adequacy of the initial linear stiffness values was evaluated using Test 010, as the multi-directional random excitation still resulted in primarily linear responses in all of the devices. Fig. 3 demonstrates that the linear stiffness estimates for Steel Damper Pair 1 from Tests 003 and 004 (shown as black lines) fit the restoring forces from Test 010 quite well. Similar figures could also be made for the sliding bearing and rubber bearing, demonstrating that those devices also evinced a good match between their estimates from Tests 003 and 004 and the measurements from Test 010. The plots in Fig. 3 also exhibit the strong similarity between the restoring forces, further emphasizing the biaxial nature of the responses. Additionally, the preliminary linear fits demonstrate that further parameters are needed to capture the dissipative components of the restoring forces.

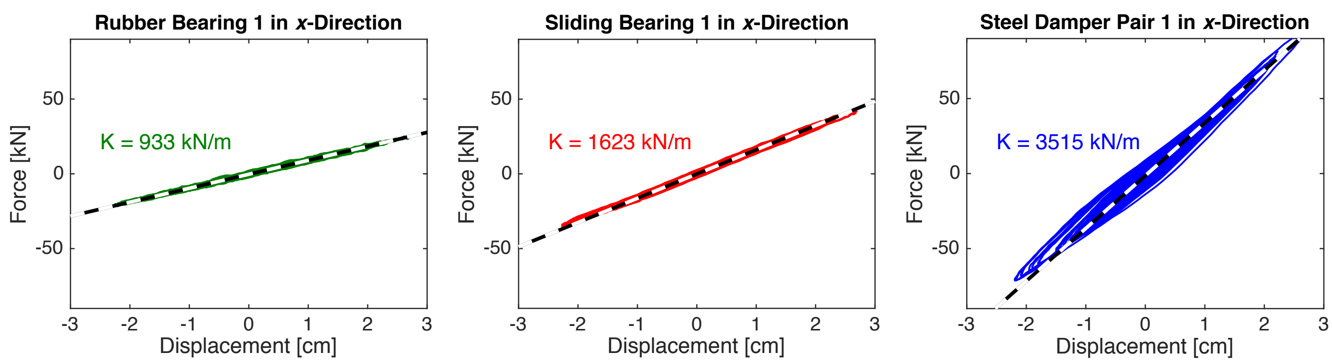

Fig. 2 – Measured restoring forces in the *x* direction for Rubber Bearing 1 (left), Sliding Bearing 1 (center), and Steel Damper Pair 1 (right) during Test 003 (random excitation along the *X* axis)

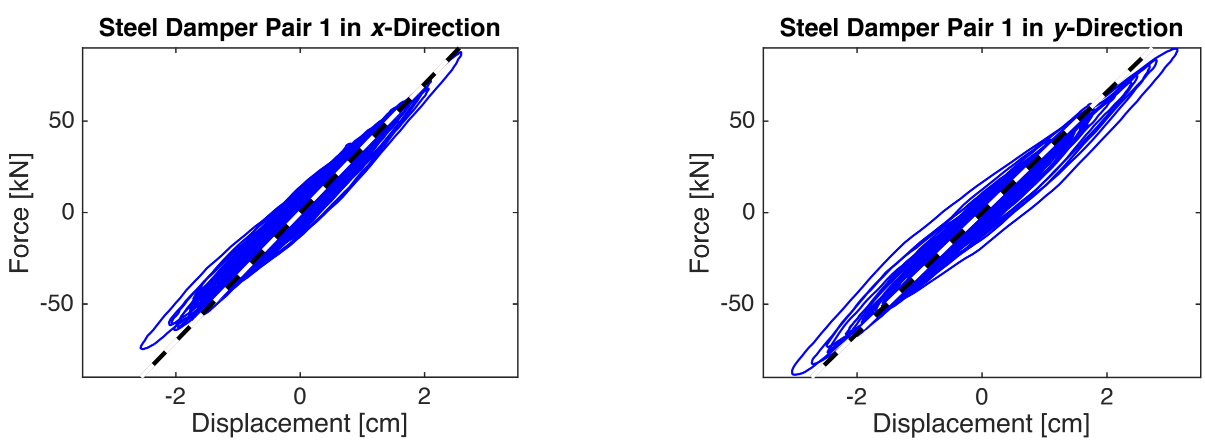

Fig. 3 – Measured restoring forces in the *x* direction (left) and *y* direction (right) for Steel Damper Pair 1 during Test 010 (random excitation across all DOFs) with preliminary linear fits (shown in black and white dashes)

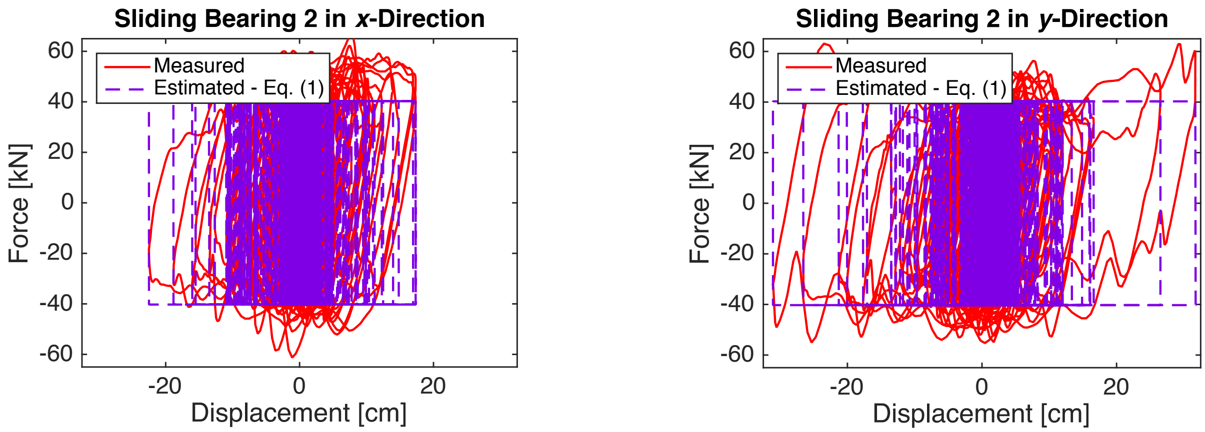

Fig. 4 – Comparison of measured and estimated restoring forces in the *x* direction (left) and *y* direction (right) for Sliding Bearing 2 during Test 016 (Tohoku earthquake) with estimates based on Eq. (1)

4.2 Seismic tests

The seismic tests elicited nonlinear, hysteretic responses from both the sliding bearings and the steel dampers. The behavior from the rubber bearing remained predominantly linear during these tests. The following subsections will detail identifying parameters for the sliding bearings and steel dampers; given that the focus of this study is on nonlinear models, the rubber bearings will not be further considered. The preliminary identification of the response from the seismic tests will be performed using measurements from Test 016, the most intense version of the scaled Tohoku earthquake tests.

4.2.1 Sliding bearings

Both models for the sliding bearings require knowledge of the sliding coefficient of friction and the bearing weight. For this structure, the nominal bearing weight — *i.e.*, the bearing weight due to the dead load of the building — was calculated based on drawings, plans, and geometry. The sliding coefficient of friction was more difficult to determine as this constant is more commonly found during targeted experimental testing [19]. As such tests were not available in this case, the coefficient of sliding friction was guessed to be $\mu_s = 0.055$ based on available measurement data and past studies [3,19].

The simple model shown in Eq. (1) was utilized in the first attempt at modeling the sliding bearing response. Based on the nominal bearing weight and assumed coefficient of sliding friction, a preliminary estimate of the restoring force was computed. However, Fig. 4 demonstrates that this model is highly insufficient. Most importantly, this simple model does not properly account for the stiffness, which can be clearly observed in the plots for both the *x*- and *y*-directional responses; therefore, modifications to the coefficient of sliding friction would not materially improve the estimate.

Based on this result, the hysteretic model was adopted and its parameters were fit using constrained nonlinear optimization. The unknown parameters for this model that would be subject to optimization were the design parameters for the hysteretic variables, A, β and γ, and the yield displacement D_y. Eqs. (3) and (4) may be reorganized to reduce the number of unknown parameters from four to three by defining new constants $\bar{A}$, $\bar{\beta}$ and $\bar{\gamma}$ using the relations shown in Eq. (7).

$$\bar{A} = \frac{A}{D_y} \qquad \bar{\beta} = \frac{\beta}{D_y} \qquad \bar{\gamma} = \frac{\gamma}{D_y} \tag{7}$$

Previous studies [2,3,19] have suggested the constraint $A = B + \gamma$, as well as $A = 1$ (and therefore $\beta + \gamma = 1$), based on viscoplasticity theory. This can be adapted such that $\bar{A} = \bar{\beta} + \bar{\gamma}$ with the added constraints that $A = 1$ and, thus, $\bar{A} > 0$, which is based on the assumption that the yield displacement D_y must be positive as well. Initial guesses for the unknown parameter vector were aided by the stiffness values found from the random excitation tests, as those stiffness values are directly related to the quantity $\mu_s W_{SB\#} \bar{A}$. Once a preliminary guess for $\bar{A}$ was quickly found, initial guesses for $\bar{\beta}$ and $\bar{\gamma}$ were chosen to be $\bar{\beta} = \bar{\gamma} = \bar{A}/2$. Utilizing the nonlinear optimization method while applying these constraints yielded the optimal predicted responses in Fig. 5. These estimates produced using Eq. (2) show noticeable improvements, especially with regards to the stiffness, relative to estimates using Eq. (1). The slope of the estimates aligns much more closely with the measurements using this equation and formulation.

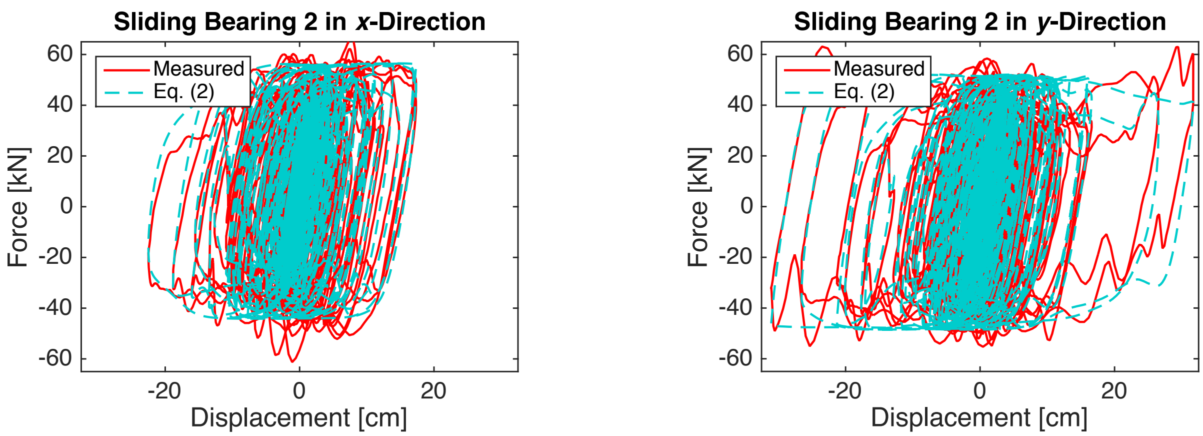

Fig. 5 – Comparison of measured and the optimally estimated restoring forces in the x direction (left) and y direction (right) for Sliding Bearing 2 during Test 016 (Tohoku earthquake) with estimates based on Eq. (2)

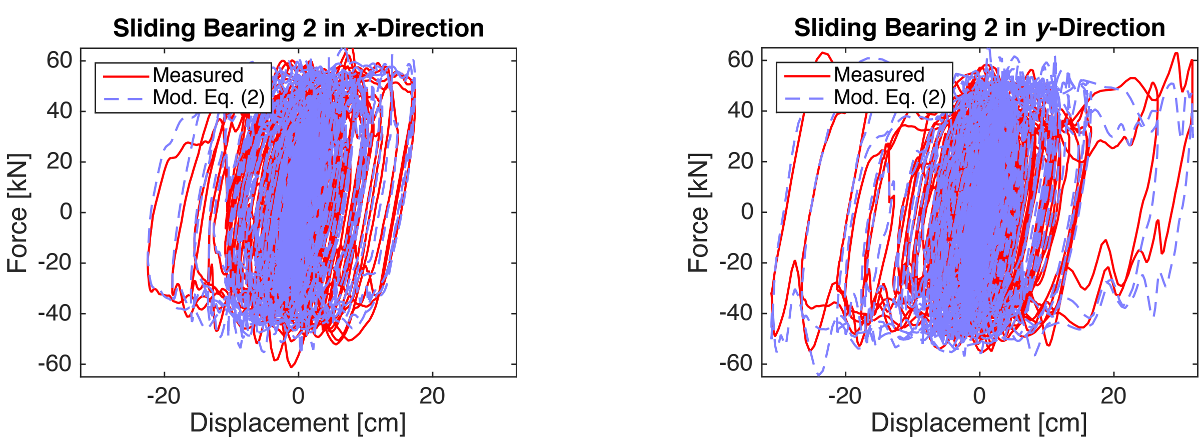

Fig. 6 – Comparison of measured and optimally estimated restoring forces in the x direction (left) and y direction (right) for Sliding Bearing 2 during Test 016 (Tohoku earthquake) using Eq. (2) with a time-varying weight

A major discrepancy remains between the measured responses and the estimates in that the measurements show fluctuations with time, oscillations not captured by the estimated model. One possible reason for this is that Eq. (2) assumes constant bearing weight. Given that this structure is asymmetric and that the isolation layer has devices of varying stiffness, as demonstrated in Fig. 1, an assumption of constant weight or pressure on the sliding bearings seems naïve; further, this ground motion has a vertical component that makes the normal force fluctuate from $W_{SB\#}$. The fluctuations in bearing weight with time may be estimated by considering the changes in normal force experienced by the sliding bearing during a test. This normal force will be equal to the weight of the structure originally apportioned to the device (the nominal bearing pressure) plus the inertial term resulting from the acceleration of the structure and the table. As the accelerations were recorded on both the table and the structure, the total acceleration experienced by the sliding bearing may be computed by finding the generalized accelerations for the base mass and then calculating the local acceleration at the sliding bearing's location.

Using this formulation changes Eq. (2) slightly such that $W_{SB\#}$ becomes a function of time, $W_{SB\#}(t)$ $W_{SB\#}(t)$. Incorporating this modification into Eq. (2) and then using the bearing weight time-history during optimization results in the optimal fit shown in Fig. 6. The fluctuations in the estimate do not perfectly match those observed in the measurements, but the modification to Eq. (2) clearly improves the qualitative match between optimal estimate and measurement without compromising the features that made the original model with Eq. (2) such an improvement over the model using Eq. (1). Including these perturbations in the bearing weight is important as their incorporation moves the model closer to replicating the real-world physical system. It is also important to note that the optimal estimates for both versions of Eq. (2) track the outer excursions of the sliding bearing quite well and generally approximate the extreme values of the restoring forces.

4.2.2 Steel dampers

The hysteretic nonlinear model for the steel dampers, originally shown in Eq. (5), includes several more unknown parameters than the model for the sliding bearing. However, the number of unknowns may be reduced using some simplifications and observations. First, as with the sliding bearing model, it will be assumed that $A = 1$, which means that, when the hysteretic components are very small (*i.e.*, near zero), the restoring force components will be directly proportional to the initial stiffness matrix and displacements. This assumption also follows the work in Park et al. [5], from where this model was originally taken.

Initial guesses for the elements of **K** can be made based on observed behavior during the random excitation tests, as shown in Figs. 1 and 2. Those plots exhibit the pre-yielding stiffness values in both the *x*- and *y*-directions. It was further assumed that **K** was symmetric and of the following form:

$$\mathbf{K} = \begin{bmatrix} k_{xx} & -k_{xy} \\ -k_{xy} & k_{yy} \end{bmatrix} \tag{8}$$

The values of k_{xx} and k_{yy} can be generally approximated from the experimental data. In works such as Narasimhan et al. [1], the cross terms k_{xy} were not included when computing the restoring forces; for this study, the cross terms are included as small but non-negligible quantities by assuming a proportional relationship with k_{xx} (as k_{xx} and k_{yy} are approximately equal), approximated as $k_{xy} = k_{xx}/10$. Finally, the post-yielding stiffness can also be estimated from the measurement data, allowing for an informed initial guess for α. These assumptions and inferences mean that, in total, only four parameters are subject to optimization: α, k_{xx}, β and γ.

The optimal parameters to fit the restoring forces measured on Steel Damper Pair 1 are then found. Fig. 7 shows that the initial parameters estimated well the pre- and post-yielding stiffness values, as was expected, but failed to capture the yielding behavior. Fig. 7 also demonstrates that the optimization algorithm was able to find parameters that provided reasonable estimates of the restoring force behavior. The fit from the optimal parameters exhibits good agreement with the measurements in both the *x* and *y* directions, proving that the bi-axial interaction was properly captured in the model. Also, as with the sliding bearings, the outer loop excursions and the extreme restoring force values are accurately estimated, which is an important consideration as these are often considered to be damage sensitive features.

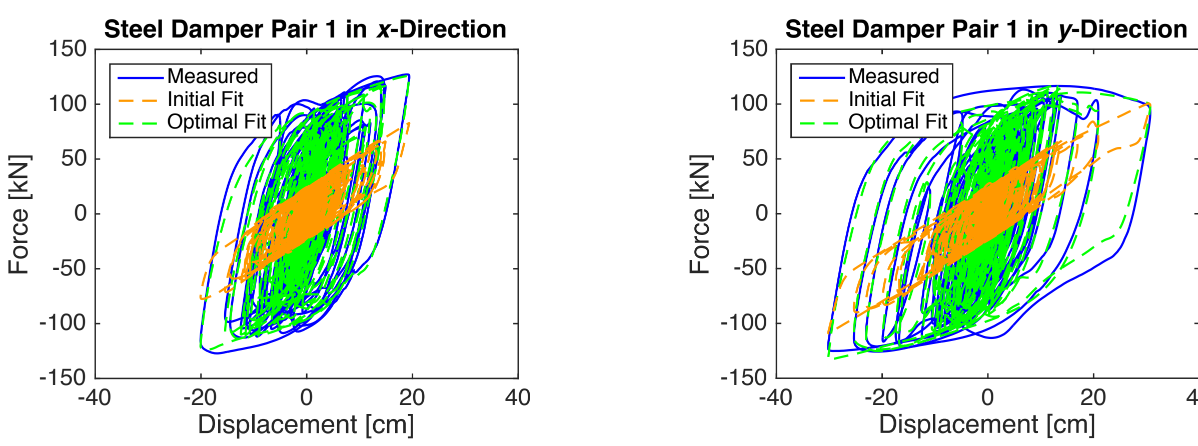

Fig. 7 – Comparison of measured, initial, and optimally estimated restoring forces in the *x* direction (left) and *y* direction (right) for Steel Damper Pair 1 during Test 016 (Tohoku earthquake)

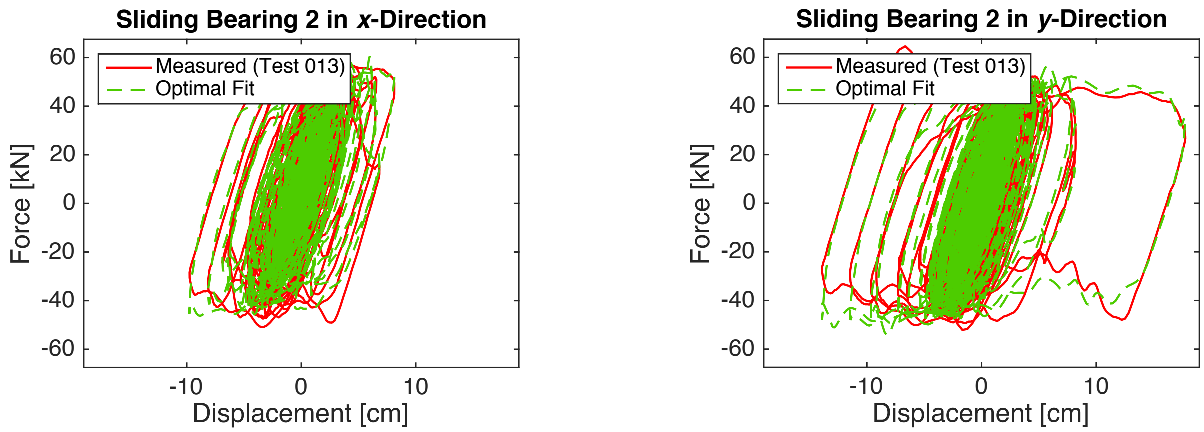

Fig. 8 – Measured restoring forces in the *x* direction (left) and *y* direction (right) from Test 013 with corresponding model estimates (using optimal params. from Test 016) for Sliding Bearing 2

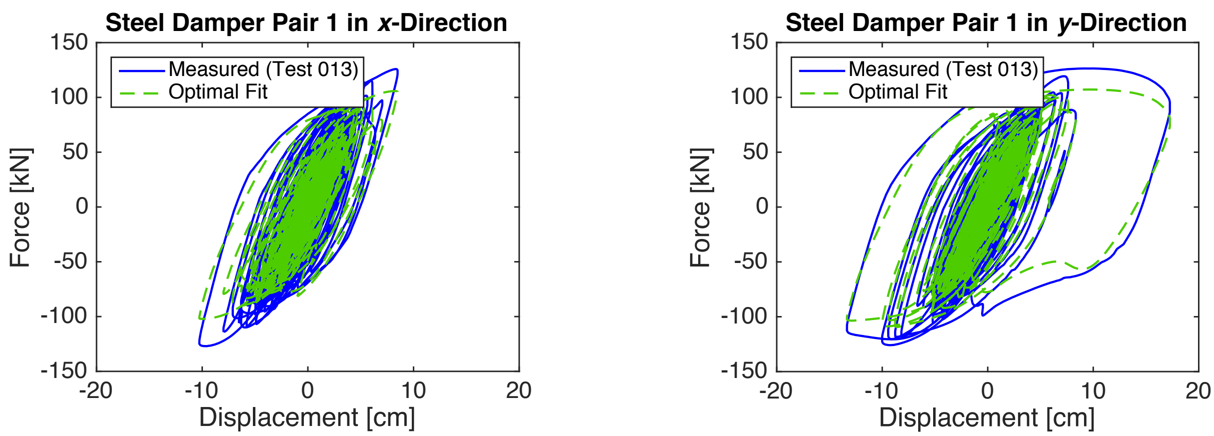

Fig. 9 – Measured restoring forces in the *x* direction (left) and *y* direction (right) from Test 013 with corresponding model estimates (using optimal params. from Test 016) for Steel Damper Pair 1

4.3 Assessing model generalizability

To determine whether the optimal models could serve as generalized models for their respective devices, the model parameters were applied to measurement data from a different seismic test to evaluate their predictive abilities. Restoring force and displacement measurements were taken from Test 013 as this was the least intense version of the Tohoku earthquake, and Table 2 showed that there was the greatest difference in RMS measurements between Test 016 and Test 013.

Fig. 8 shows that the sliding bearing model using the modified version of Eq. (2) provides a reasonable prediction of the restoring force in both the *x* and *y* directions. This demonstrates that the sliding bearing model is capable of capturing and predicting fully biaxial hysteretic responses. As with the fitted model, the slopes, outer loops, and extreme values also match well between the measurements and predictions.

The predictions for the steel damper pair are shown in Fig. 9, demonstrating that this model also provides accurate and reliable predictions of biaxial interactions. However, comparing Figs. 8 and 9 reinforces how the model of the steel damper better captures the real behavior than does the sliding bearing model.

Another important indicator of generalizability is whether the model parameters identified from one device may be applied to a similar device. The measurement data from Test 016 of the complementary devices (Sliding Bearing 1 and Steel Damper Pair 2) are compared to the predictions of the models (which were calibrated from Test 016 data of Sliding Bearing 2 and Steel Damper Pair 1). It was assumed that using data from the same test but the opposite device would provide a fair comparison. Fig. 10 shows that the model for

Sliding Bearing 2 provides an extremely poor prediction of the restoring force of Sliding Bearing 1, demonstrating that Sliding Bearing 1 did not behave in a manner similar to Sliding Bearing 2. These two devices were clearly governed by different physical interactions during this test, as evidenced by the sharp transitions in the restoring force of Sliding Bearing 1 that are more indicative of "sticking/releasing" cycles rather than "slipping" behavior. These stark differences in physical behavior mean that the model was probably an inadequate choice from the start.

The steel dampers behaved in a much more congruous manner, as the restoring force evinced by Steel Damper Pair 2, shown in Fig. 11, is very similar to Steel Damper Pair 1 in Fig. 7. This similarity greatly contributed to the model's ability to provide accurate predictions of the restoring forces for the other steel damper. The predictions for Steel Damper Pair 2, despite not being used for fitting, are nearly as accurate as those for Steel Damper Pair 1. Also, the damage sensitive features, *e.g.*, outer loops and restoring force extrema, are also captured, which is a consistent trend for the steel damper model across different tests and devices.

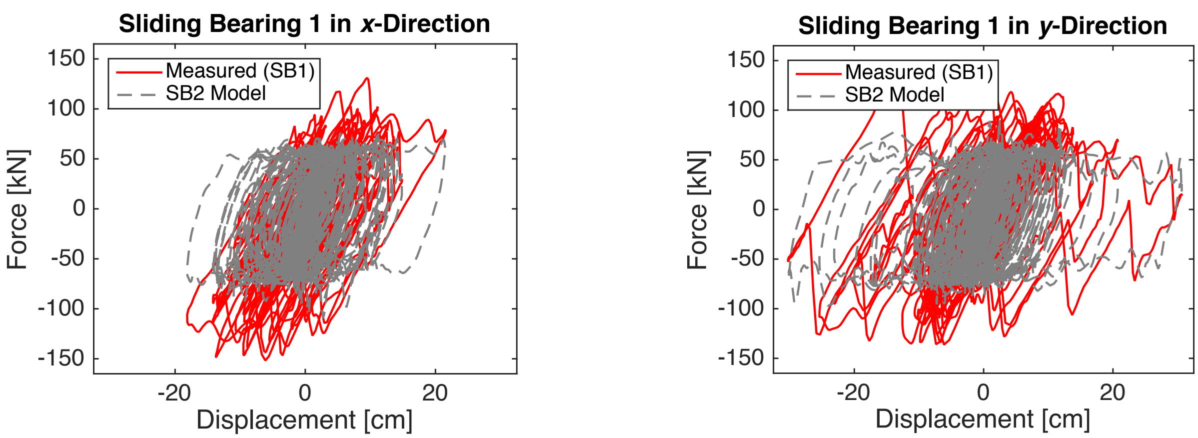

Fig. 10 – Measured restoring forces in the x direction (left) and y direction (right) with corresponding model estimates for Sliding Bearing 1 (using optimal params. from Sliding Bearing 2) from Test 016

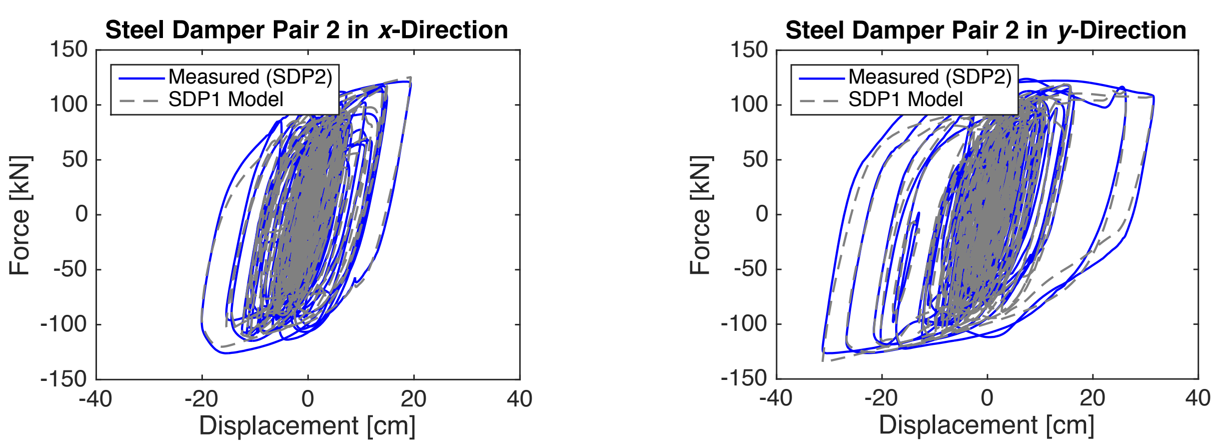

Fig. 11 – Measured restoring forces in the x direction (left) and y direction (right) with corresponding model estimates for Steel Damper Pair 2 (using optimal params. from Steel Damper 1) from Test 016

5. Conclusions

Biaxial hysteretic models were able to capture and reproduce the nonlinear behavior observed in the restoring forces of elastic sliding bearings and steel yielding dampers during large-scale testing of a base-isolated building subjected to earthquake excitation. For each device, the unknown coefficients in its model were determined via nonlinear optimization. The optimal parameters for each model produced a good fit of the observed restoring force behavior. It was also revealed that the model of the steel damper could serve as a generalized model, predicting the responses to other seismic tests and for the other steel damper, but the model of one sliding bearing could predict responses for other tests for the same bearing but not for the other bearing. This was due to the fact that the both steel dampers behaved in a similar manner during testing, whereas the sliding bearings exhibited disparate response behaviors. Most importantly, the steel dampers behaved in a manner that generally conformed to the assumed model, whereas the sliding bearing required a modified model that likely still failed to properly capture the complex physics and interactions present in the devices.

With this in mind, future studies should continue to investigate the limits of both models. For the steel dampers, this means determining if the model may be generalized to include seismic excitations beyond scaled versions of the same earthquake, such as those with similar spectral characteristics but different time histories, as well as those with widely different characteristics. For the sliding bearings, further exploration and development of a model that can properly capture the variations in bearing pressure is necessary, as these fluctuations may be the result of design considerations that are regularly encountered in real world structures, *e.g.*, asymmetric loading, non-homogeneity in the base-isolation layer, multi-directional and multi-component seismic inputs, etc. Additionally, the sticking behavior observed in the other sliding bearing should be investigated in terms of whether the current models, if tuned correctly, can capture that behavior and make reliable predictions. Creating reliable and accurate generalized models of seismic protective systems is of high value to the structural and earthquake engineering communities, and, thus, all avenues of inquiry must be pursued as each new results enable smarter and safer designs against the challenges and risks posed by natural hazards.

Acknowledgments

This material is based upon work supported by the National Science Foundation under Grants CMMI 13-44937/ 13-44622 and 14-46424/14-46353; any opinions, findings, and conclusions or recommendations expressed in this material are those of the authors and do not necessarily reflect the views of the National Science Foundation. The first author gratefully acknowledges the support of the Viterbi Postdoctoral Fellowship from the University of Southern California.

References

[1] Narasimhan S, Nagarajaiah S, Johnson EA, Gavin HP (2006): Smart base-isolated benchmark building part I: problem definition, *Structural Control and Health Monitoring*, **13**(2-3), 573-588.

[2] Nagarajaiah S, Reinhorn AM, Constantinou MC (1991): Nonlinear dynamic analysis of 3-D–base-isolated structures, *ASCE Journal of Structural Engineering*, **117**(7), 2035-2054.

[3] Mokha AS, Constantinou MC, and Reinhorn AM (1993): Verification of friction model of Teflon bearings under triaxial load, *ASCE Journal of Structural Engineering*, **119**(1), 240-261.

[4] Furukawa T, Ito M, Izawa K, Noori MN (2005): System identification of base-isolated building using seismic response data, *ASCE Journal of Engineering Mechanics*, **131**(3), 268-275.

[5] Park YJ, Wen YK, Ang AH-S (1986): Random vibration of hysteretic systems under bi-directional ground motions, *Earthquake Engineering & Structural Dynamics*, **14**(4), 543-557.

[6] Sato E, Sasaki T, Fukuyama K, Tahara K, Kajiwara K (2013): Development of innovative base-isolation system based on E-Defense full-scale shake table experiments part I: outline of project research. *AIJ Annual Meeting*, Hokkaido, Japan, (in Japanese).

[7] Ibrahim, RA (2008): Recent advances in nonlinear passive vibration isolators, *Journal of Sound and Vibration*, **314**(3-5), 371-452.

[8] Hwang JS, Chiou (1996): An equivalent linear model of lead-rubber seismic isolation bearings, *Engineering Structures*, **18**(7), 528-536.

[9] Lomiento G, Bonessio N, Benzoni G (2013): Friction model for sliding bearings under seismic excitation, *Journal of Earthquake Engineering*, **17**(8), 1162-1191.

[10] Mosqueda G, Whittaker AS, Fenves GL (2004): Characterization and modeling of friction pendulum bearings subjected to multiple components of excitation, *ASCE Journal of Structural Engineering*, **130**(3), 433-442.

[11] Landi L, Grazi G, Diotallevi PP (2016): Comparison of different models for friction pendulum isolators in structures subjected to horizontal and vertical ground motions, *Soil Dynamics and Earthquake Engineering*, **81**, 75-83.

[12] Harvey Jr. PS, Gavin HP (2015): Assessment of rolling isolation system using reduced order structural models, *Engineering Structures*, **99**, 708-725.

[13] Moreschi LM, Singh MP (2003): Design of yielding metallic and friction dampers for optimal seismic performance, *Earthquake Engineering & Structural Dynamics*, **32**(8), 1291-1311.

[14] Ene D, Kishiki S, Yamada S, Jiao Y, Konishi Y, Terashima M, Kawamura N (2016): Experimental study on the bidirectional inelastic deformation capacity of U-shape steel dampers for seismic isolated buildings, *Earthquake Engineering & Structural Dynamics*, **45**(2), 173-192.

[15] Benedettini F, Capecchi D, Vestroni F (1995): Identification of hysteretic oscillators under earthquake loading by nonparametric models, *ASCE Journal of Engineering Mechanics*, **121**(5), 606-612.

[16] Yar M, Hammond J (1987): Parameter estimation for hysteretic systems, *Journal of Sound and Vibration*, **117**(1), 161-172.

[17] Peng C, Iwan W (1992): An identification methodology for a class of hysteretic structures, *Earthquake Engineering & Structural Dynamics*, **21**(8), 695-712.

[18] Ni YQ, Ko JM, Wong CW (1998): Identification of non-linear hysteretic isolators from periodic vibration tests, *Journal of Sound and Vibration*, **217**(4), 737-756.

[19] Constantinou M, Mokha A, Reinhorn A (1990): Teflon bearings in base isolation. II: modeling, *ASCE Journal of Structural Engineering*, **116**(2), 455-474.

[20] Wen YK (1980): Equivalent linearization for hysteretic systems under random excitations, *ASME Journal of Applied Mechanics*, **47**(1), 150-154.